Astronomy
&
Astrophysics

Shock-induced PDR in the Herbig-Haro object HH 2

B. Lefloch[1], J. Cernicharo[2], S. Cabrit[3], and D. Cesarsky[4]

[1] Laboratoire d'Astrophysique de l'Observatoire de Grenoble, BP 53, 38041 Grenoble Cedex, France
    e-mail: lefloch@obs.ujf-grenoble.fr
[2] Consejo Superior de Investigaciones Científicas, Instituto de Estructura de la Materia, Serrano 123, 28006 Madrid, Spain
[3] LERMA, Observatoire de Paris, UMR 8112, France
[4] Max-Planck Institut für Extraterrestrische Physik, 85741 Garching, Germany

Abstract. We report mid-infrared (5–17 μm) and SO, CO, ^{13}CO millimeter line observations of the protostellar jet HH 2 and the parental molecular cloud. We have detected for the first time mid-infrared emission along a protostellar jet. We find that the outflowing gas extends much further away than the Herbig-Haro object HH 2, showing direct evidence that downstream gas has been accelerated by previous outflow events. These gas layers appear to have been detached from the parental cloud, as they are distributed around a cavity, probably dug by protostellar outflow(s). SO emission is detected in shocked gas regions associated with outflows. The UV field produced in the strong shock region HH 2H-A has produced a low-excitation Photon-Dominated Region at the walls of the cavity, which is detected in the PAH emission bands and in the continuum between 5 and 17 μm. This continuum arises from very small grains transiently heated by a FUV field G $\simeq$ 20 G_0, which probably formed from evaporation of dust grain mantles in shocks.

Key words. ISM: Herbig-Haro objects – ISM: individual objects: HH 1/2 – ISM: jets and outflows – ISM: dust, extinction – stars: formation

1. Introduction

The Herbig-Haro system HH 1–2 is one of the best-studied star forming region. It attracted early attention because of the spectacular shock emission regions HH 1 and HH 2 that trace the interaction of the protostellar jet with the ambient cloud. This jet is characterized by rather high velocities in the ionic and atomic material (up to 480 km s^{-1}) and large proper motions in the impact region, as measured with HST (Bally et al. 2002). The optical jet is associated with a molecular outflow, first mapped in CO by Moro-Martín et al. (1999). The jet makes a strong inclination angle with the line of sight ≈80°. The high-velocity, collimated component of the outflow (the "molecular jet") covers deprojected velocities of 15−80 km s^{-1}. This system was first studied by Martin-Pintado & Cernicharo (1987) who suggested that the spatial distribution of the molecular emission resulted from the interaction of the outflowing jet with the ambient molecular cloud, producing cavities and density enhancements along the walls of these cavities.

In the HH 2 region, the impact in the ambient gas results in shocks with a wide range of velocities: from 20−30 km s^{-1} in the rim, corresponding to the individual knots E-K (Lefloch et al. 2003) up to 180 km s^{-1} in the Mach disk region, which was identified as the optical knots HH 2H-2A. Observations in the UV (Boehm-Vitense et al. 1982; Raymond et al. 1997) and X-ray (Pravdo et al. 2001) show extended emission from this shock region.

There has been a long debate as to whether such a high-energy field would have any noticeable impact on the local surroundings. Based on previous molecular line observations, the gas downstream of HH 2 appears to be in a quiescent state. However, Davis et al. (1990) report an enhanced abundance of HCO$^+$ in that region. Torelles (1992) obtained a similar result for NH$_3$. A detailed study by Girart et al. (2002) revealed the peculiar chemical composition of the molecular emission peak in the region downstream of HH 2: some molecules were found largely overabundant (CH$_3$OH, H$_2$CO, HCO$^+$, SO, SO$_2$) and others, like CS and HCN, were underabundant. These features appeared to agree qualitatively with chemical models of UV-irradiated gas clumps (Wolfire & Königl 1993; Viti & Williams 1999), which predict large abundance enhancements in a wide variety of molecular species, from either purely gas phase reactions or the release from icy grain mantles. Time-dependent modelling by Viti et al. (2003) could account for *some* of the molecular abundances measured by Girart et al. (2002), paying special attention to the HCO$^+$ emission. Other observational evidence of the impact of the UV field on the ambient gas around HH 2 came from the observation of the FIR lines [CII] 158 μm and [OI] at 63 and 145 μm with ISO/LWS at 80″ resolution by Molinari & Noriega-Crespo (2002). They found that shock models cannot account for the line intensities measured and concluded that at least part of the emission must arise from a PDR associated with HH 2, but lack of angular

resolution prevented any further characterization. Their modelling also made the assumption that the PDR is excited mainly by 2γ UV photons.

On the other hand, it is well established that shocks can strongly alter the chemical composition in the entrained gas of protostellar outflows (see e.g. Bachiller & Perez-Gutierrez 1997). Indeed, recent $HCO^+ J = 1 \rightarrow 0$ interferometric observations by Dent et al. (2003) reveal a high-velocity component moving along HH 2. The authors conclude that the observed HCO^+ abundance enhancement is consistent with shock chemistry in the turbulent mixing layer associated with the jet.

In this article, we reassess the nature of the molecular emission around HH 2, from $5-17$ μm spectro-imaging observations of the HH 2 region obtained with the ISOCAM camera onboard ISO and complementary observations of millimeter transitions of CO, ^{13}CO and SO, at the IRAM 30 m telescope, paying special attention to the position studied by Girart et al. (2002), which we will refer to as the "molecular emission peak". Our observations show HH 2 to be even more complex than initially thought. We find that previous outflow episodes have accelerated gas ahead of HH2 and have dug a cavity in the parental cloud. Shocked gas is detected along the walls of the cavity. The mapping of SO emission shows that it is associated with the shock interaction of the outflowing gas with the parental cloud. The strong J-type shocks associated with HH 2H-A have induced the formation of a Photon-Dominated Region (PDR) at the inner wall of the cavity, which could be mapped and characterized in the mid-IR.

2. Observations

The CO and ^{13}CO millimeter line data were obtained at the IRAM 30m telescope and have been presented and discussed in Moro-Martín et al. (1999), hereafter MM99.

The SO transitions 3_4-2_3 at 138.17864 GHz and 2_3-1_2 at 99.299883 GHz were observed with the IRAM 30m telescope in March 1993. The observing conditions were very good, with typical system temperatures of 180–200 K at 2mm. The angular resolution of the telescope is $17''$ and $24''$, respectively, at these frequencies. An autocorrelator with a spectral resolution of 20kHz was used as a spectrometer. The data was smoothed to obtain a kinematical resolution of ≈ 0.05 km s^{-1}. The SO emission was mapped with a $15''$ sampling over a region of about $200''$ by $200''$ centered on the VLA 1 source. The flux is expressed in units of main-bream brightness temperature. The efficiency of the telescope was 0.65 and 0.55 at 99.299883 GHz and 138.17864 GHz respectively.

The mid-infrared observations were obtained with the ISO satellite (Kessler et al. 1996) and the ISOCAM instrument (Cesarsky et al. 1996). The low resolution spectra ($\lambda/\Delta\lambda = 40$) between 5 and 17 μm were obtained in revolution 691 with the Circular Variable Filter (CVF) with a pixel scale of $6''$ and a total field of view of $3'$ centered on the HH 2 object. We present the data reduced with the pipeline version OLP10. The size (HPFW) of the Point Spread Function (PSF) is $\approx 6''$ for a pixel scale of $6''$.

Accurate astrometry (better than $2''$) was established using a second CVF map containing the optically visible Cohen-Schwartz (CS) star, taken in revolution 873. Details are given in Cernicharo (2000) and Lefloch et al. (2003). The zodiacal light and a possible large-scale emission across the field were suppressed by subtracting a reference spectrum from the whole dataset. A spectrum of the residual emission, away from HH 2, is shown in panel A of Fig. 8c (the "empty field"). In addition to the CVF map we obtained an image of the flux integrated in the range 5.0−8.5 μm, including the H_2 pure rotational lines S(8)–S(4) and the PAH bands at 6.2 and 7.7 μm. We extracted a map of the continuum emission in the range 13.9−15.5 μm, outside the interval of emission of the [Ne 2], [Ne 3] and H_2 S(2) lines. The data are presented in Fig. 8. Coordinates are offsets (arcsec) relative to the position of VLA1: $\alpha_{2000} = 05^h36^m22.6^s$, $\delta_{2000} = -06°46'25''$.

The SNR of the data is not very high; we have averaged the signal over four fields typical of the region, which are drawn in Fig. 8: in the cloud (A), along the jet (D), and over the "ring" (B,C, see below). The interstellar extinction towards HH 2 was estimated by Hartmann & Raymond (1984), who measured typical reddenings $E(B - V) = 0.11-0.44$. Based on the extinction curve of Rieke & Lebofsky (1985), it appears that the flux dereddening corrections are negligible and we use uncorrected flux values in what follows.

3. Entrained gas in the HH 2 region

Although the region has been extensively studied and several outflows identified (see e.g. Chernin & Masson 1995; Correia et al. 1997) it is only recently (1999) that the molecular counterpart to the HH 1–2 jet was discovered (Moro-Martin et al. 1999). The confusion in the HH 2 region is indeed very high; because of the weakness of the outflow emission and a propagation close to the plane of the sky (about 10°, Noriega-Crespo et al. 1991), it is difficult to identify the different kinematical components in line spectra.

Several observations suggest that the medium in front of HH 2 has been accelerated in the past. Henney et al. (1994) showed that the medium in front of the counterjet of HH 2 (HH 1) is moving at a considerable velocity, 200 km s^{-1}. Ogura (1995) reported the presence of two giant bowshocks symetrically located at 30 arcmin from the protostellar core and aligned with HH 1–2, ejected some 10^4 yr ago. These bowshocks were interpreted as the signature of previous ejections from the source powering the HH 1–2 jet. We have re-analyzed more thoroughly the ^{12}CO data presented by MM99 to search for any hint of outflow/ejections older than the HH 1–2 jet mapped by them.

3.1. A CO outflow ahead of HH 2

We show in Fig. 1 the CO $J = 2 \rightarrow 1$ high-velocity gas emission in the HH 2 region, as mapped by MM99. The *redshifted* ($v_{lsr} = 12-16$ km s^{-1}) outflow wing associated with the HH 2 jet extends between the driving source VLA 1 and the HH object (the H_2 knots of shocked gas are marked by white stars in Fig. 1. Close inspection of the data reveals another CO component, well collimated, which propagates downstream of the red wing at *blueshifted* velocities ($v_{lsr} = 2-4$ km s^{-1}).
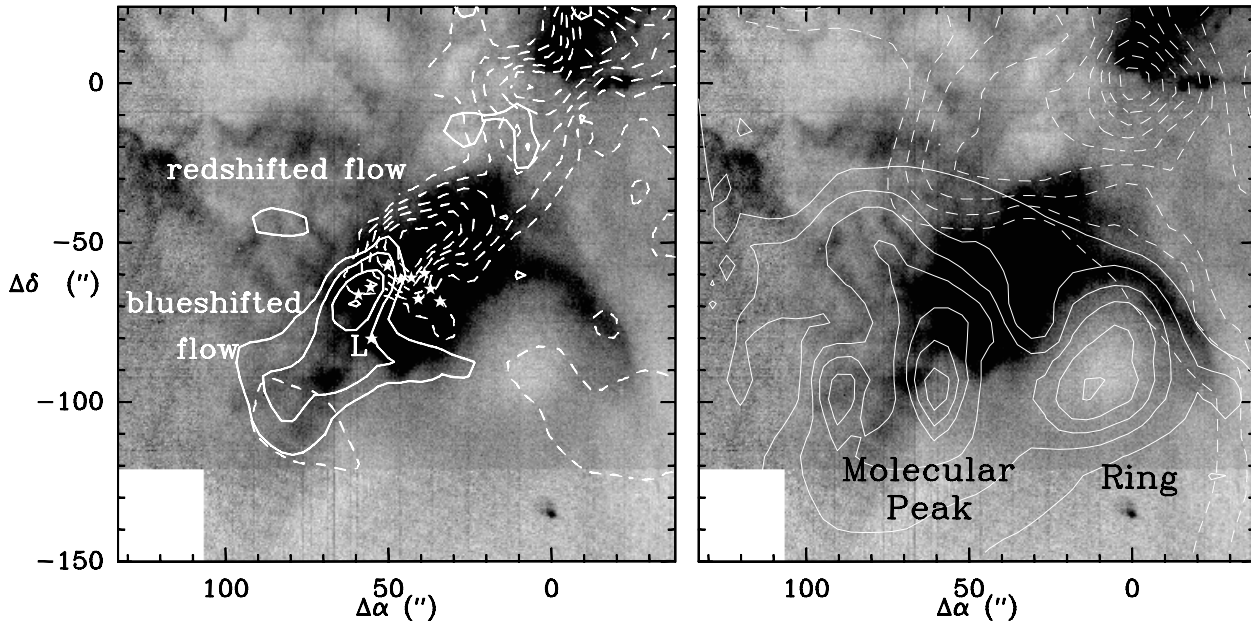
Fig. 1. *(Left)* Map of the high-velocity outflow emission in the $^{12}CO(2-1)$ line (thick black contours) superposed on the map of the $^{13}CO(2-1)$ emission (thick white contours) and a [SII] image of the region (greyscale; Reipurth et al. 1983). The image has been saturated to outline the ring and the weak emission downstream of HH2. The redshifted wing of the HH 2 outflow is drawn in dashed contours. Contours range from 4 to 20 K km s^{-1} by step of 2 K km s^{-1}. The blueshifted wing is drawn in solid contours. First contour and contour interval are 1 and 0.5 K km s^{-1} respectively. The white stars mark the position of the HH 2 knots A to L. The position of the regions discussed in the text (the "ring" and the molecular emission peak downstream HH 2) are indicated. *(Right)* Map of the $^{13}CO(2-1)$ emission integrated between 5.5 and 6.75 km s^{-1} (thick white contours) and between 9.5 and 12 km s^{-1} (dashed) superposed on a [SII] image of the region (greyscale). Intensity contours range from 6 to 11 K km s^{-1}.

A spectrum of the CO outflowing gas near the brightness peak at offset position (60″, −75″) is displayed in Fig. 2. The blueshifted wing overlaps very well the ambient gas layers, as traced by ^{13}CO. The maximum of brightness in the blue component is detected in the region that coincides with the HCO$^+$ high-velocity wing reported by Dent et al. (2003). This kinematical component extends from knots HH 2 K-E and propagates over ≈50″, ahead of knot L (see Fig. 1). The optical [SII] emission of HH 2 reveals a faint jet that propagates ahead of HH 2 and coincides spatially with the CO blueshifted outflow (see left panel in Fig. 1). This jet is likely to be the driving source of the blueshifted molecular material.

A crude estimate of the parameters in the outflowing gas was made by assuming a kinetic temperature of 30 K. As can be seen in Fig. 2, the CO spectra indicate antenna temperatures of ≃20 K, which is a lower limit to the intrinsic line brightness. The brightness temperature of the very optically thick CO lines provides a lower limit to the actual gas kinetic temperature, which is about 25 K. An upper limit is provided by the main-beam brightness temperature ≃40 K; we adopt an intermediate value of 30 K in this work. This value is characteristic of the ambient gas and may underestimate the actual temperature in the outflowing gas. It is higher than the 13 K estimated by Girart et al. (2002). These authors obtained this estimate indirectly, based on a multi-transition Monte-Carlo analysis of HCO$^+$. We favor our approach, which relies directly on the observation of a "standard" tracer; excitation problems can be very severe for HCO$^+$. The presence of a thermal gradient in the layers cannot be excluded, in which case the temperature
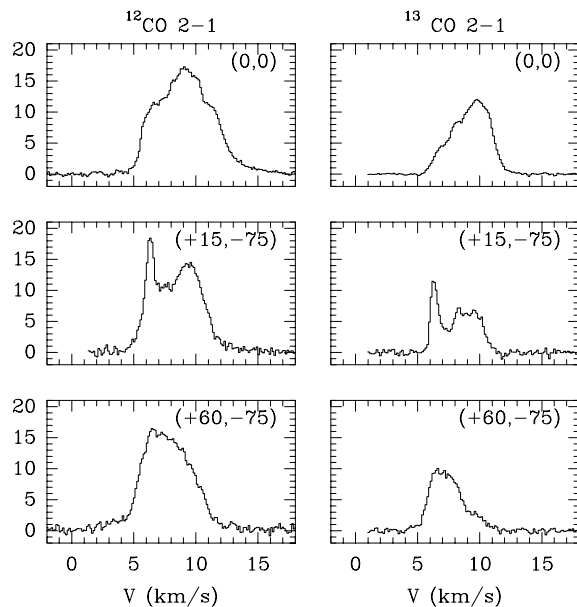

Fig. 2. Montage of $^{12}CO(2-1)$ and $^{13}CO(2-1)$ spectra at 3 positions: the protostellar core (*top*), the "ring" (*middle*), and the "molecular peak" downstream of HH 2 (*bottom*).

at the surface (traced by the low-excitation CO line) could be higher than in the inner denser regions probed by HCO$^+$.

Integrating the wing emission in the range 2−4 km s^{-1}, we find a mass of 0.015 $M_\odot$ and a momentum of 0.1 $M_\odot$ km s^{-1}. These parameters compare well with those derived for the
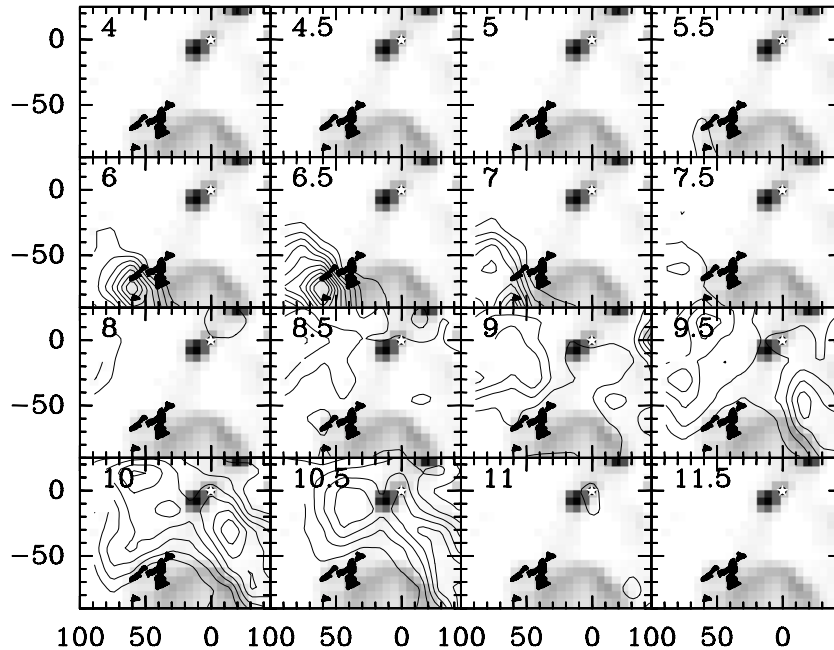
Fig. 3. Velocity-integrated intensity channel map of the SO 3_4-2_3 emission in the HH 1–2 region (contours), superposed on the 5.0–8.5 μm emission map obtained with ISO. First contour and contour interval is 0.2 K. Velocity is indicated in the top left corner of each panel. The position of VLA 1 is marked by a white star. The individual HH knots are drawn in black. Coordinates are in arcsec offset with respect to VLA 1.

high-velocity molecular outflow associated with the HH 2 jet. This blueshifted component appears relatively well collimated and is aligned with the *redshifted* Herbig-Haro jet HH 2, which suggests a common origin for both ejections. Both components slightly overlap at the position of the knots E-F-K, where the maximum of shocked H_2 emission is detected in the mid-IR (Lefloch et al. 2003). The alignment and overlap is better seen in the higher-angular resolution observations of Dent et al. (2003). Though appealing, it is not clear if this change of orientation results from precession of the jet driving source (blue and red components would be tracing two different ejections) or from deflection upon impact on dense obstacle (the components are tracing one single jet). Both components have approximately the same (projected) size $\approx 50'' = 3.3 \times 10^{17}$ cm, and could trace two ejections separated by 500 yr, assuming a typical ejection velocity of 200 km s^{-1}. This blueshifted outflow and the optical jet downstream of HH 2 provide direct evidence that material ahead of HH2 has already been accelerated by previous outflowing ejections.

3.2. The high-density gas emission

SO is a tracer whose emission is more highly contrasted than CO because its abundance can be greatly enhanced in shocks and in the high-temperature central protostellar regions (the "hot cores" of low- and high-mass protostars), where grain mantles are evaporated and S-bearing molecules released in the gas phase. SO is therefore especially suited to map the shocked gas of the outflow and its interaction with the ambient cloud. We detected extended SO emission over the entire surveyed region. We show in Fig. 3 a channel map of the velocity-integrated flux of the SO 3_4-2_3 line. We found two maxima; the first one is located at position ($-75''$, $12''$), the second one lies

very close to knot HH 2L at position ($60''$, $-75''$), in very good agreement with the "molecular peak" position determined by Girart et al. (2002). At this position, SO lines are bright (~ 4 K), more than twice as bright as in the protostellar core, where the HH 1 jet is detected as a blue wing, and in the HH 2 outflow (see Fig. 4).

We concentrate on the region downstream HH 2 in what follows. From the half-power contour, we estimate a transverse (deconvolved) size of $\approx 20''$, hence barely resolved by our observations. We show in Fig. 4 the profiles obtained in a 4-point cut in declination across the brightness peak at ($60''$, $-75''$). The line profiles peak at about 6.5 km s^{-1}. However, they are characterized by several kinematical components, which vary between adjacent positions, separated by 15$''$. At $\delta = -90''$, a secondary component is detected at 6.89 km s^{-1}. The velocity channel map suggests that the 7 km s^{-1} component peaks at lower declination, near position ($50''$, $-90''$). Unfortunately, the data sampling is lower in that region (30$''$) and does not allow us to resolve details in the structure of this feature. North of the peak ($\delta > -60''$), a secondary component is detected at 10 km s^{-1}. It is is rather weak, with $T_{mb} \sim 1$ K, but it is unambiguously detected across the whole map. It is spatially associated with low-redshifted gas which extends from the VLA 1 protostellar core to HH 2 and beyond. Overall, the gas traced by SO does not appear quiescent in the region downstream of HH 2.

3.2.1. Physical properties of the SO emission

We have carried out an LVG analysis of the SO emission at a few positions close to the brightness peak region, considering one single gas component. We have neglected any thermal and/or density gradients in the emitting gas layer, despite the
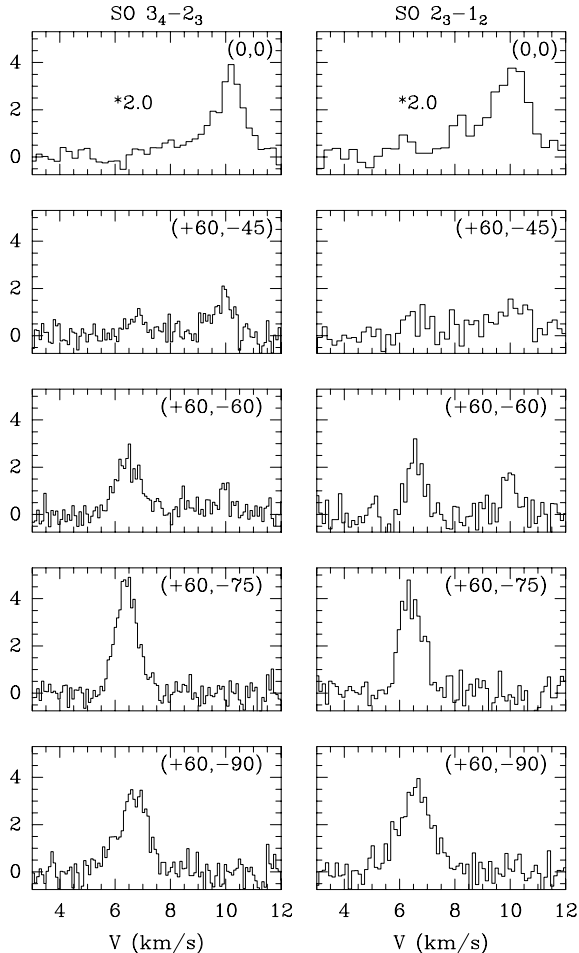
Fig. 4. Spectra of the SO 3_4-2_3 and 2_3-1_2 lines observed towards the molecular emission peak downstream HH 2 at offset position $(60''$, $-75'')$ and the protostellar source VLA 1. Flux is in main-beam brightness temperature. Line intensities have been multiplied by 2.0 for the VLA 1 spectra.
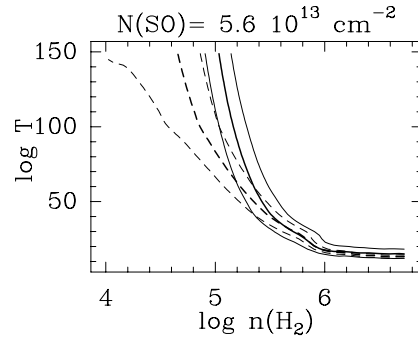

Fig. 5. Variations of the SO $3_4-2_3/2_3-1_2$ (thick solid) and $6_7-5_6/5_6-4_5$ (thick dashed) intensity line ratios with temperature and density at the molecular peak. The SO column density is taken to be 5.6×10^{13} cm^{-2} (see text). Thin contours draw the values at 90 and 110.

fact that the SO emission arises from a shocked gas layer, as we discuss below in Sect. 3.2.2. Taking into account such an effect would introduce an additional degree of freedom in the modelling, for which the present observational data set does not bring any constraints. We adopt a kinetic temperature of 30 K, similar to that determined in the lower-density gas traced by CO (see above). Collisional rates for SO have been derived from those of CS-H$_2$ computed by Green & Chapman (1978); the procedure for $^3\Sigma$ molecules is described by Fuente et al. (1990). We obtained very similar results using the more recent collisional rates computed by Green (1994) and extrapolated at temperatures lower than 50 K.

At the peak, both lines are bright with main beam temperatures of 4.2 K and 4.7 K for the 2_3-1_2 and 3_4-2_3 transitions respectively. Linewidths are ≈ 1 km s^{-1}. We find a solution for a column density $N(\text{SO}) = 5.6 \times 10^{13}$ cm^{-2} and a gas density $n(\text{H}_2) = 5.5 \times 10^5$ cm^{-3}. The lines are optically thin with opacities of 0.45 and 0.23 for the 3_4-2_3 and 2_3-1_2 respectively. The LVG calculations predict intensities of 2.2 K for the 5_6-4_5 219.9494 GHz and 0.91 K for the 6_7-5_6 261.8437 GHz, both transitions observed by

Girart et al. (2002) at the SO peak. This is in good agreement with the line brightness, once corrected for the beam dilution factor (respectively 0.257 and 0.322).

We note that a lower temperature, of the order of 15 K for the emitting gas, would require much higher densities, of the order of $n(\text{H}_2) = 5 \times 10^6$ cm^{-3}, and $N(\text{SO}) \simeq 6.5 \times 10^{13}$ cm^{-2}. These densities are far too high and lead to a flux much larger than what is observed for the 5_6-4_5 and 6_7-5_6 transitions (2.7 K and 1.3 K respectively). These results differ somewhat from the simple LTE analysis by Girart et al. (2002). Indeed, the excitation temperature ranges from 24 K for the 2_3-1_2 transition down to 9 K for the 6_7-5_6 transition, showing that these transitions are far from being thermalized.

Taking into account the uncertainties in the brightness determination, it appears that various sets of physical conditions can account for the observed lines. We have explored the range of solutions in the parameter space defined by the density and the temperature, adopting the SO column density determined above at the brightness peak (the "best solution"). We show in Fig. 5 the intensity line ratios $3_4-2_3/2_3-1_2$ (thick solid line) and $6_7-5_6/5_6-4_5$ (thick dashed line). A good agreement is obtained for densities in the range $3-6 \times 10^5$ cm^{-3} and temperatures between 25 and 40 K. Allowing a variation of 10% for each ratio, we find that the density has to be more than 10^5 cm^{-3}, and the temperature less than 100 K. If the density $n(\text{H}_2)$ is larger than 2.5×10^5 cm^{-3} i.e. the average gas density in the layer (see Sect. 4.1), the temperature is relatively well constrained, between 20 K and 60 K. Observations of higher-excitation transitions of SO (and CO) would help constrain the temperature.

Comparison of the relative intensities at the neighbouring positions (Fig. 4) shows that the 3_4-2_3 intensities is lower than 2_3-1_2, suggesting a change of excitation conditions, namely a lower density. An LVG analysis yields a column density $N(\text{SO}) = 3.0-4.0 \times 10^{13}$ cm^{-2} and a density $n(\text{H}_2) \simeq 2 \times 10^5$ cm^{-3}. If the gas temperature were lower, typically 15 K, the densities derived would be $n(\text{H}_2) \simeq 6-7 \times 10^5$ cm^{-3}, which is very unlikely for structures with a size of 10^{17} cm in the molecular cloud. The densities derived from our LVG approach are very similar to those quoted by Dent et al. (2003),
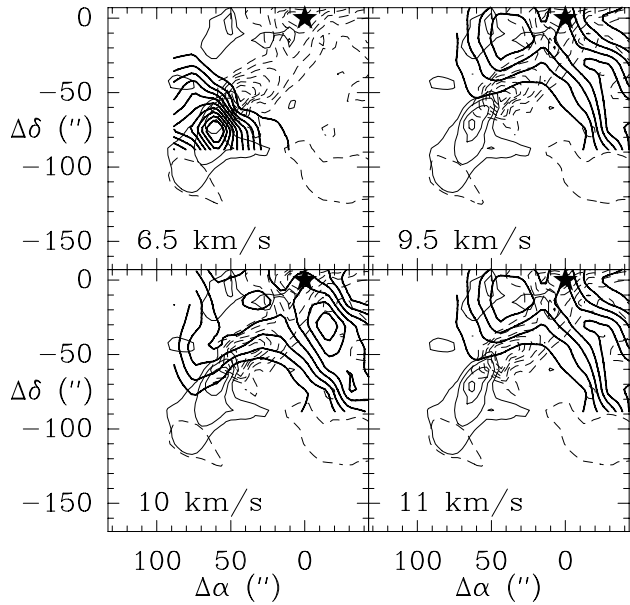
Fig. 6. Comparison of the emission distribution of the SO 3_4-2_3 (black contours) at various velocity intervals (6.5, 9.5, 10, 10.5 km s^{-1}) with the CO 2–1 high-velocity outflow. First contour and contour interval are 0.2 K.

from millimeter dust continuum, and from modelling of the HCO$^+$ emission by Girart et al. (2002).

The secondary component at 10 km s^{-1} detected North of the SO peak ($\delta = -60''$ and $\delta = -45''$) is characterized by high-excitation conditions with a ratio $3_4-2_3/2_3-1_2 \sim 1.5$. Such a high value is found only at the SO emission peak ahead of HH 2 (it is less than 1 elsewhere in that area). Carrying out an LVG analysis of the position ($60''$, $-45''$) and adopting a kinetic temperature of 30 K, we find a gas density $n(H_2) = 5 \times 10^6$ cm^{-3} and $N(SO) = 2.0 \times 10^{13}$ cm^{-2}. Again, the density estimate relies on the temperature adopted, but we stress that 30 K is probably a reasonable lower limit (lower temperatures require even higher densities, $\sim 10^7$ cm^{-3}, irrealistically large for the large-scale entrained gas of a molecular outflow). The emitting gas is therefore characterized by high densities, much larger than in the ambient parental cloud, and possibly warmer temperatures. Taking into account that this gas is moving into the ambient cloud, we conclude that at least part of the SO component is tracing gas shocked and/or accelerated by the HH 2 jet.

3.2.2. Origin of SO emission

How does the distribution of the SO-emitting gas relate to the CO outflowing gas detected in HH 2? Figure 6 shows that SO traces the large-scale features associated with the accelerated gas detected in CO on each side of the protostellar core at 8.5 km s^{-1}. In the protostellar core itself, the SO line profiles exhibit blue- and red-shifted wings, which are the signature of the HH 1–2 outflow. We did not find any evidence of emission *along* the jet down to HH 2; instead, we detect in the same velocity range emission that is spatially shifted with respect to the jet; such a shift could be an indication that the emission arises from the jet rim, i.e. the low-velocity shock region of the jet

(see Lefloch et al. 2003). The gas column densities derived are indeed comparable to the values encountered in other young protostellar outflows, like L1157 (Bachiller & Perez-Gutierrez 1997). Observations at higher-angular resolution would help clarify this point.

As discussed above, the high-velocity blushifted outflow propagates into the gas layers downstream of HH 2, where SO is detected at velocities equal or very close to ambient (Fig. 6). The SO emission is elongated perpendicular to the CO outflow direction, which propagates across the SO region -limited by the contour at half-power- and finishes $\approx 40''$ Southeast of the SO peak. Both ambient SO and high-velocity CO brightness peaks are very close to each other (less than $10''$) and to knot HH 2L, where shocked molecular gas is detected (see e.g. Lefloch et al. 2003). This peak coincides with the maximum of density and of SO column density. Analysis of the physical conditions shows that the gas is denser than in the ambient parental cloud and could be warmer than the 30 K estimated from CO. The detection of high-velocity gas at the position where the density is highest suggests that SO is tracing the impact of the flow in the cloud. Also, the amount of SO material detected along the HH 2 jet and the layers downstream of HH 2 are similar (to less than a factor of 3), which suggests a common mechanism, and the column densities derived are typical of protostellar outflows.

Because the inclination of the flow with respect to the line of sight is very large, it is difficult to determine at which velocity SO emission occurs when the flow impacts the gas layers. Detailed modelling would help constrain the physical conditions of the shock that could account for the SO emission detected or if on the contrary UV radiation plays an important role in the emission detected.

4. A cavity in the cloud

In the previous section, we showed evidence that the protostellar outflow from VLA 1 has propagated beyond HH 2. Its impact on the ambient gas causes shocks which are detected in high-density tracers such as SO. Previous studies of the gas and dust structure in multiple star forming regions suggest that flows can have some other impact on the cloud dynamics; the study of NGC 1333 revealed for instance the presence of cavities in the cloud, apparently dug by the protostellar outflows (see e.g. Lefloch et al. 1998). We study in this section the large-scale distribution of the molecular gas kinematics around HH 2, to search for any similar impact of the outflowing gas on the parental cloud.

4.1. The low-density gas around HH 2

We have studied the distribution of the low-density molecular gas by mapping the emission of the ^{13}CO(2–1) line. We present in Fig. 7 the map of the velocity-integrated flux in the range 5−11 km s^{-1}. Three regions can be distinguished depending on the strength of the emission: the ambient cloud, between 8 and 9 km s^{-1}; a fragment downstream of HH 2, between 5 and 8 km s^{-1}; the "filament" southwest of the protostellar core, between 10 and 11 km s^{-1}.
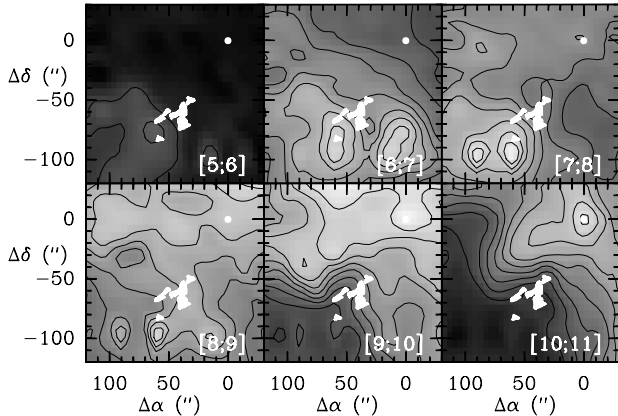
Fig. 7. Map of the velocity-integrated ^{13}CO(2–1) intensity in the HH 2 region. First contour and contour interval are 2 and 1 K km s^{-1} respectively. Velocity interval is indicated in the bottom right corner. The invidual HH knots are drawn in white.

We do not find any evidence of a large-scale velocity gradient in the cloud. The velocity field in the cloud and the "filaments" are rather smooth. The latter overlaps very well with the border of the cloud. On the contrary, there is a striking morphological association between the layers at blue velocities (5−8 km s^{-1}) and the ambient cloud (see right panel in Fig. 1): the integrated emission of the fragment matches exactly the border of the ambient cloud, which is possible only because there is barely any ambient emission.

We detect two local maxima in the fragment downstream of HH 2: one coincides with the "molecular emission peak" and the other peaks at the center of the optical "ring" at offset position (15″, −90″) (see Fig. 8d). The gas in the fragment peaks at ≈ 6.3 km s^{-1}. The emission is characterized by bright lines ($\sim$10 K) with a narrow linewidth ($\sim$1 km s^{-1}; see offset position (15″, −75″) in Fig. 2).

An LVG calculation performed with a temperature of 30 K gives a column density $N(H_2) \simeq 6.0 \times 10^{21}$ cm^{-2} at both positions in the layers. We note that the line opacity is quite high ($\simeq 0.68$); it is probably the reason for the lack of contrast in the emission. The gas column density derived is in rough agreement with the determination obtained by Dent et al. (2003), who found $N(H_2) = 2 \times 10^{22}$ cm^{-2} at the peak from dust millimeter continuum observations. From the mean H_2 density in the gas ($\sim 2 \times 10^5$ cm^{-3}), we find that the thickness of the emitting region is ~ 3–6×10^{16} cm (5″−10″), much smaller than the extent over the sky. The emission appears to be distributed in a sheet of dense gas rather than in a "round clump". This means that the dense "ambient" gas emission is distribued around a cavity.

4.2. Shocked H$_2$ around the cavity

Our ISOCAM/CVF observations (Fig. 8d) reveal some weak H$_2$ emission in the S(2) and the S(3) lines above the 4σ level in the gas shell where the second ^{13}CO maximum is detected – offset position (15″, −90″). The H$_2$ emission is detected at the border of the gas layer, where the extinction is

much less ($A_v \simeq 4$ at the molecular peak). The maximum of absorption in the center of the gas shell at (15″, −90″)) is responsible for the annular appearance of the structure.

The H$_2$ emission follows the distribution of the mid-infrared continuum and the 11.3 μm PAH band. The CVF spectra obtained towards the ring are similar to those of low-excitation galactic Photon Dominated Regions, such as Chamameleon, which are exposed to a low FUV field of a few ten times the ISRF (Boulanger et al. 1998). In none of the galatic PDRs of similar excitation conditions has H$_2$ been detected. Therefore, we conclude that the S(2) and S(3) lines are tracing shocked gas over the shell. The non-detection of higher-J H$_2$ transitions suggests low-excitation conditions, perhaps due to low-velocity shocks or previous (old) shocks. This strengthens our hypothesis that the shell of dense gas has been shaped by shocks, most likely from outflows.

It is therefore no wonder that the mid-IR emission map shows no correlation with the millimeter thermal dust emission, which traces the "cold" dust. This component is detected mainly in the protostellar condensation VLA 1–4 and in the layers ahead of HH 2 (Dent et al. 2003). The ring and the jet coincide with a minimum in the "cold" dust emission. Conversely, the maximum of absorption in the layer ahead of HH 2 prevents any mid-IR radiation from escaping the border of the cavity.

4.3. Dust grain properties

The dust grains in the ring exhibit properties very different from those observed in the protostellar envelopes of VLA 1–4. In the ring, we do not find any evidence *at all* of the presence of mantle ices. The silicate absorption is so large towards VLA 1 that it makes it difficult to analyse the mantle composition. The lower absorption in the envelope of VLA 4 allows us to characterize the composition of the mantle ices: H_2O, CH_3OH, CH_4, CO_2 (Cernicharo et al. 2000). A broad bump from 11 to about 14 μm is detected all over the ring. Such a bump is interpreted as the signature of crystalline silicates, although the exact composition would require complementary data at longer wavelengths. Note that crystalline silicates have also been detected around the CS star (Cernicharo et al. 2000). Standard dust grains are expected to undergo deep changes in their composition when crossing shock(s) in the protostellar jet, as they release their icy mantle into the gas phase, either because of sputtering or shattering (Jones et al. 1994). Such processes result in an enrichment of the population of very small grains. Most likely, the very small grains detected by ISOCAM in the jet and in the ring are the result of this enrichment. In this context, a simple explanation for the detection of crystalline silicates is that they were originally present in grain *cores* and had already started to crystallize before the mantles evaporated. Further spectroscopy with the instruments onboard SPITZER should allow us to better constrain the composition and the physical parameters of the dust grains. As discussed above, the peculiar gas composition ahead of HH 2 most likely results from shock(s) too. Molecular line observations at higher angular resolution should be undertaken to better constrain the parameters of the shock.
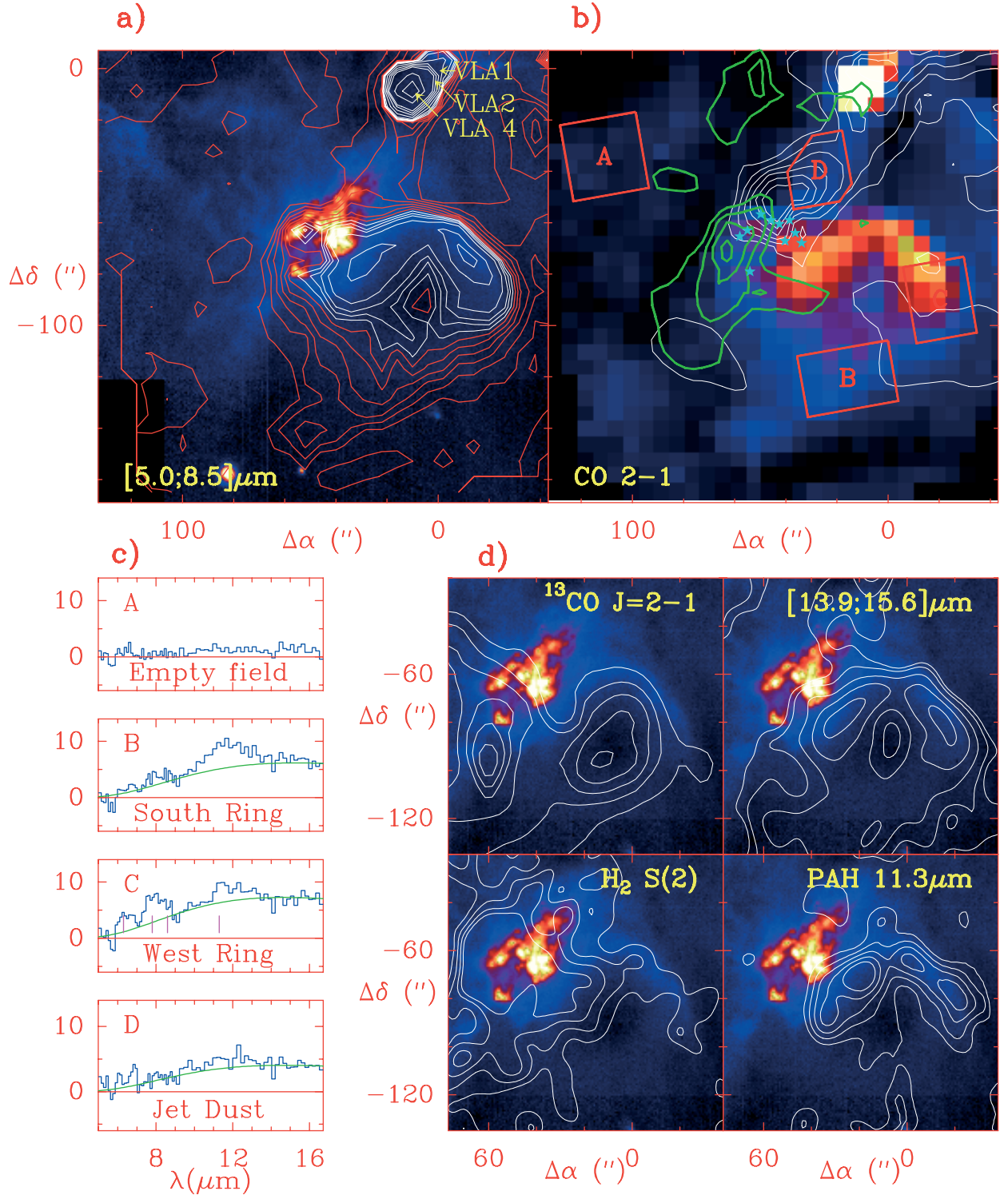
Fig. 8. a) Mid-infrared emission integrated between 5 and 8.5 μm superposed on an optical [S 2] image of HH 2 (Reipurth 1993). Contours range from 3 to 5.6 mJy by step of 0.2 mJy/pixel (px), from 6 to 10 mJy by step of 1 mJy/px, from 15 to 20 mJy by step of 5 mJy/px. **b)** High-velocity CO $J = 2 \rightarrow 1$ emission (white contours) superposed on the 5.0−8.5 μm integrated mid-infrared map (colourscale). Contours range from 4 to 20 K km s^{-1} by step of 2 K km s^{-1}. The position of the individual shocks A-L are marked with stars. Red polygons delineate the fields used to compute individual spectra. **c)** Spectra of the mid-infrared emission between 5.0 and 17 μm. **d)** Emission detected towards the "ring" West of HH 2H in: ^{13}CO(2–1): contours range from 6 to 11 K km s^{-1} by step of 1 K km s^{-1}; H$_2$ S(2) 12.2 μm: contours range from 4 to 10 mJy by step of 2 mJy/px; 13.9−15.4 μm continuum: first contour is 4 mJy, following contours range from 4.5 mJy to 7.5 mJy by step of 1 mJy/px; PAH 11.3 μm band: contours range from 2 to 4.5 mJy by step of 0.5 mJy/px. The CVF maps were convolved with a Gaussian of 12″ HPFW to outline the extended emission. The rms in the 11.3 μm PAH map and the continuum map is 0.3 mJy/px; it is ≈1 mJy/px in the H$_2$ S(2) map.

4.4. What is the origin of the cavity?

The peculiar geometry of the gas fragment downstream of HH 2 suggests that it could have been detached from the parental cloud. At least two observational facts suggest that the outflow activity could be responsible for detaching this fragment. First, the border of the ambient cloud coincides with the location of the knots HH 2A-K, where violent, dissociative shocks are detected. Second, the outflow wing downstream of HH 2 coincides very well with the gas fragment, in the plane of the sky. Both gas components (the fragment and the outflow wing) are *blueshifted* with respect to the ambient cloud.

On the other hand, the momentum carried away by the blueshifted outflow wind is $\approx 0.1 \, M_\odot \, \mathrm{km \, s^{-1}}$, i.e. a factor of a few less than the momentum necessary to detach the fragment from the cloud. The sum of several ejections in the past could have provided enough momentum; we speculate that another outflow, much more powerful, could be responsible for digging the cavity in the ambient cloud. When looking at the velocity channel map of SO emission (Fig. 3), it is interesting to note that the filament southwest of the core: a) consists of dense gas (SO); b) is velocity-shifted with respect to the ambient cloud; c) closely follows the border of the latter. Such a configuration is suggestive of a shock front propagating from the border of the cavity into the cloud. The orientation of such an outflow would probably be closer to North-South than the actual HH 1–2 jet.

5. Photon-Dominated Region in HH 2

The emission integrated between 5 and 17 μm is shown in Figs. 8a, b. The SNR rms is ~0.1 mJy in the map. Protostar VLA 4 (Cernicharo et al. 2000) is detected as a bright point source in Figs. 8a, b. After subtracting the contribution of the ambient cloud, estimated from a reference position, the residual flux appears very weak; a spectrum of the emission averaged over a reference field centered at $(+100'', -35'')$ shows a contribution less than ~1 mJy (panel A in Fig. 8c). Hence, the emission discussed here arises from the HH 2 region. Southeast of the protostellar core down to HH 2, we detect mid-infrared emission *along the HH 2 jet*. The average flux level was estimated over field D and is about 5 mJy longwards of 10 μm (5σ above the rms noise level). The spatial coincidence with the CO high-velocity outflow (Fig. 1) suggests a physical association with the latter. The nature of the CVF emission appears to be mainly continuum in the jet, as indicated by the spectrum of Field D (Fig. 8c). This is the first time that mid-infrared *continuum* emission is reported towards a protostellar jet.

The map of the pure continuum between 13.9 and 15.4 μm shows that most of the flux comes from a ring-like structure (hereafter the "ring") of 60$''$ diameter (0.13 pc), westwards of HH 2H (Fig. 8d), This annular structure is detected in the optical SII line (Reipurth et al. 1993) and in the 5.0−8.5 μm emission map. The minimum of emission in the center of the ring coincides with the peak of gas column density detected in ^{13}CO, at offset position $(15'', -75'')$. This provides direct evidence that the mid-IR "ring" and the molecular gas surrounding the cavity are closely related. The average spectrum of the ring obtained in field C shows the emission of the UIBs between 6.2 and 11.3 μm, which are a direct tracer of the local UV field. Identification is more difficult in the Southern part of the ring (field B); the SNR is not high enough to conclude about a gradient in the PAH abundance. However, the continuum emission detected in the South testifies to the fact that the whole gas layer is illuminated by UV photons, on the rear side.

The emitting region, as traced by the 11.3 μm map (Fig. 8d), coincides very well with the pure continuum emission distribution. In the jet, on the contrary, we note that there is no hint of PAH emission bands. The relatively low SNR and the strong cloud extinction prevent us from drawing a conclusion about the presence/absence of PAHs along the jet.

A rough estimate of the FUV field intensity is obtained by integrating the flux in the ISOCAM band. This yields an infrared luminosity $L \sim 0.01 \, L_\odot$, and a FUV field: $G = 20 \, \mathrm{G_0}$. This is fully consistent with the estimate obtained by Molinari & Noriega-Crespo (2002) from the analysis of the FIR [CII] 158 μm and [OI] 63 μm, 145 μm lines and the FIR continuum observed at 80$''$ resolution with ISO/LWS. We note that our direct estimate of the FUV lies in the low range of values (20–1000 $\mathrm{G_0}$) required by the models of UV-driven photochemistry (Viti et al. 2003) to account for the molecular emission ahead of HH 2.

Continuum emission in the jet and the ring could be fitted by a greybody with an opacity law $\tau_\nu \propto \nu$ and a temperature $T_\mathrm{d} = 200-250 \, \mathrm{K}$. Assuming that the emission comes from typical interstellar a(big) dust grains, we find that the amount of material corresponds to an $A_\mathrm{v} \simeq 0.1-1 \times 10^{-6}$, which translates into very low gas column densities. The efficiency of dust grains with a size as small as 0.003 μm is too low (Draine & Lee 1984) to reach equilibrium temperatures of this order, unless the UV field is actually very strong, far above our estimate. Most likely, we are observing the emission of very small dust grains, transiently heated to high temperatures by the local UV field.

Weak continuum flux is also detected across the HH object and West of the protostellar core VLA 1–4. This extension coincides with the border of the cavity in the molecular cloud.

5.1. HH 2H as exciting source of the PDR

Previous observations in the UV have revealed strong extended emission in the direction of HH 2H-2A (Böhm-Vitense et al. 1982; Raymond et al. 1997). The other sources in the field detected by IUE are HH 1 and the Cohen-Schwartz star; both are located too far away to account for the PDR observed around HH 2. Analysis of optical high-ionization lines has shown evidence for a *J*-type shock with velocities of ~180 km s^{-1} moving into previously accelerated gas (optical measurements indicate proper motions up to 400 km s^{-1} towards HH 2H and HH 2A (Bally et al. 2002), identifying HH 2H as the actual jet impact region (or Mach disk region). HH 2H-2A is therefore the most plausible candidate as an exciting source; it is also the only place where X-ray emission has been detected in the region (Pravdo 2001).

HUT measurements by Raymond et al. (1997) show that the UV continuum is dominated by 2 photon radiation of collisionally excited H atoms longwards of 1750 Å. At shorter wavelengths, the continuum is dominated by H_2 Lyman emission bands. Once corrected for the interstellar extinction, the total UV luminosity is $\sim 0.3\ L_{\odot}$; it is distributed roughly equally between both mechanisms. The exact solid angle encompassed by the ring is difficult to estimate. Following our hypothesis that the outflow has dug a cavity around HH 2, it is reasonable to assume that the ring and the molecular emission peak ahead of HH 2 are at about the same distance to the UV source, knots H-A (50″). The diameter of the ring is 60″, hence the fraction of photons intercepted by the ring is $\sim 5\%$, which compares well with the mid-IR luminosity radiated by the very small grains in the walls of the cavity (3% of the UV luminosity produced in HH2H-2A).

The possibility of a similar mechanism (strong J-shocks) to account for the mid-infrared emission along the protostellar jet, between VLA 1 and HH 2, should be explored. Deep sensitive spectroscopy of the entrained gas could allow one to constrain such possibility. Another possibility is that the jet region is actually almost free of dust grains after the crossing of the strong shocks which are now impacting HH 2. In this case we would be detecting the walls of a dust-free cavity around the *jet*, illuminated either by HH 2H or by the powering source.

6. Summary and conclusions

The observations presented in this paper allow us to draw a more complete and complex picture of the HH 2 region. In addition to the high-velocity molecular outflow associated with the optical jet HH 1–2, we have detected another outflow component that propagates over 50″ in the molecular gas downstream HH 2. This outflow is associated with a weak jet detected in the optical, which appears to come from HH 2. The orientation of this component in the sky differs from the HH 2 jet and could be the result of jet deflection on the dense obstacles responsible for the knots of H_2 emission in HH 2. Another possibility is that this component traces a previous ejection from the source, which would be precessing. High angular resolution observations should allow us to test the first hypothesis, by comparison with numerical modelling (see e.g. Raga & Canto 1995)

This provides direct evidence that the molecular gas ahead of HH 2 has been affected by protostellar ejections. It is consistent with the detection of optical bow-shocks at large distances from the HH 1–2 region. Several kinematical components are detected in the gas downstream of HH 2. Observations of SO sreveal the presence of very dense gas ($\sim 2-5 \times 10^5$ cm^{-3}) associated with the low-velocity shocks along the HH 2 jet, and in the blueshifted outflow, close to knot HH 2L. The latter position coincides with the peak of emission in the region. We conclude that SO is probably tracing the shock interaction of the outflow with the ambient gas.

The gas layers downstream of HH 2 exhibit evidence of shocks: East of HH 2, ISOCAM observations detect H_2 line emission in the gas layers, which is the signature of shocks, probably old enough to be detected only in the low-excitation

transitions S(2) and S(3). The gas layers have been shaped in a shell, probably as the result of prostellar outflow interaction with the cloud. Actually, the morphology and kinematics of the filament Southwest of the protostellar core are compatible with their tracing a shock-compressed"back side" of the cavity (the "front side" being the gas shell downstream of HH 2).

ISOCAM observations show emission from very small grains at the inner surface of the cavity downstream of HH 2. This could result from the shattering and sputtering of large interstellar dust grains in the outflow/cloud interaction. We find that the UV field produced in the strong shock HH 2H-A, which illuminates the inner side of the cavity, creates a Photon-Dominated Region of FUV intensity $G \sim 20\ G_0$. It is sufficient to account for the emission of the very small grains and the PAHs detected. Mid-infrared emission along the jet remains a puzzle; deep mid-infrared spectroscopy along the jet could allow one to determine the origin of the emission, in particular if it is related to strong dissociative shocks between the source and HH 2.

Our observations indicate that some of the molecular species whose abundance is found enhanced in the gas downstream of HH 2 are actually produced in the region of outflow interaction with the cloud. Mapping at better angular resolution, comparable to the data presented here, should be undertaken. In combination with detailed shock modelling, it would allow us to explore the shock hypothesis and estimate its relative contribution with respect to UV-induced photodesorption in the gas phase enrichment of "unusual" molecular species.

References

Bachiller, R., & Perez Gutierrez, M. 1997, ApJ, 487, L93
Bally, J., Heathcote, S., Reipurth, B., et al. 2002, ApJ, 123, 2667
Böhm-Vitense, E., Böhm, K. H., Cardell, J. A., & Nemec, J. M. 1982, ApJ, 262, 224
Boulanger, F., Abergel, A., Bernard, J. P., et al. 1998, in Star Formation with the Infrared Space Observatory, ed. J. Yun, & R. Liseau ASP Conf. Ser., 132, 15,
Cernicharo, J., Noriega-Crespo, A., Cesarsky, D., et al. 2000, Science, 288, 649
Cesarsky, C. J., Abergel, A., Agnese, P., et al. 1996, A&A, 315, L32
Davis, C. J., Dent, W. R. F., & Bell Burnell, S. J. 1990, MNRAS, 244, 173
Dent, W. R. F., Furuya, R. S., & Davis, C. J. 2003, 339, 633
Draine, B. T., & Lee, H. M. 1984, ApJ, 285, 89
Fuente, A., Cernicharo, J., Barcia, A., & Gomez-Gonzalez, J. 1990, A&A, 231, 151
Girart, J. M., Viti, S., Williams, D. A., Estalella, R., & Ho, P. T. P. 2002, A&A, 388, 1004
Green, S. 1994, ApJ, 434, 188
Green, S., & Chapman, S. 1978, ApJS, 37, 169
Hartmann, L., & Raymond, J. C. 1984, ApJ, 276, 560

Henney, W. J., Raga, A. C., & Axon, D. J. 1994, ApJ, 427, 305

Hester, J. J., Stapelfeldt, K. R., & Scowen, P. A. 1998, ApJ, 116, 372

Hollenbach, D., & McKee, C. F. 1989, ApJ, 342, 306

Jones, A. P., Tielens, A. G. G. M., Hollenbach, D. J., & McKee, C. F. 1994, ApJ, 433, 797

Kessler, M. F., Steinz, J. A., & Anderegg, M. E. 1996, A&A, 315, L27

Lefloch, B., Cernicharo, J., Cabrit, S., et al. 2003, ApJ, 590, L41

Martin-Pintado, J., & Cernicharo, J. 1987, A&A, 176, L27

Molinari, S., & Noriega-Crespo, A. 2002, ApJ, 123, 2010

Moro-Martín, Cernicharo, J., Noriega-Crespo, A., & Martín-Pintado, J. 1999, ApJ, 520, L111 (MM99)

Ogura, K. 1995, ApJ, 450, L23

Pravdo, S. H., Feigelson, E. D., Garmire, G., et al. 2001, Nature, 413, 708

Raga, A. C., & Cantó, J. 1995, RmxAA, 31, 51

Rieke, G. H., & Lebofsky, M. J. 1985, ApJ, 288, 618

Raymond, J., Blair, W. P., & Long, K. S. 1997, ApJ, 489, 314

Reipurth, B., Heathcote, S., Roth, M., Noriega-Crespo, A., & Raga, A. C. 1993, ApJ, 408, L408

Torelles, J. M., Rodriguez, L. F., Canto, J., et al. 1992, ApJ, 396, 95

Viti, S., & Williams, D. A. 1999, MNRAS, 310, 517

Viti, S., Girart, J. M., Garrod, R., et al. 2003, A&A, 399, 187

Wolfire, M. G., & Königl, A. 1993, ApJ, 415, 204